



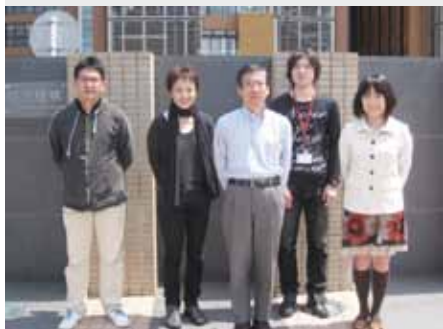
RESEARCH ACTIVITIES

Life and Coordination-Complex Molecular Science

Department of Life and Coordination-Complex Molecular Science is composed of two divisions of biomolecular science, two divisions of coordination-complex molecular science, and one adjunct division. Biomolecular science divisions cover the studies on the elucidation of functions, dynamic structures, and mechanisms for various biomolecules such as sensor, membrane, and metal proteins, glycoconjugates, and molecular chaperone. Coordination complex divisions aim to develop molecular catalysts and functional metal complexes for transformation of organic molecules, reversible conversion between chemical and electrical energies, and artificial photosynthesis. Interdisciplinary alliances in this department aim to create new basic concepts for the molecular and energy conversion through the fundamental science conducted at each division.

Bioinorganic Chemistry of Metal-Containing Sensor Proteins

Department of Life and Coordination-Complex Molecular Science
Division of Biomolecular Functions



AONO, Shigetoshi
YOSHIOKA, Shiro
SAWAI, Hitomi
YAMANAKA, Masaru
TANIZAWA, Misako

Professor
Assistant Professor
IMS Research Assistant Professor
Post-Doctoral Fellow
Secretary

Heme shows many biological functions. The most popular function is to be used as a prosthetic group in heme proteins. Heme proteins show a variety of functions including oxygen transport/storage, electron transfer, oxidase, peroxidase, oxygenase, catalase, and dehydratase. In addition to these functions, a new function of heme protein has been found recently, which is a sensor of diatomic gas molecules or redox change.^{1,2)} In these heme-based sensor proteins, the heme acts as the active site for sensing the external signal such as gas molecules and redox change. Heme also shows a novel biological function as a signaling molecule for transcriptional and translational regulation. In these systems, heme-sensing proteins sense a heme molecule to regulate biological processes. Our research interests are focused on the elucidation of the structure-function relationships of these heme-based sensor proteins and heme-sensing proteins.

1. Bacterial Gas Sensor Proteins Using Transition Metal-Containing Prosthetic Groups as Active Sites³⁾

Gas sensor proteins are involved in many biological regulatory systems, including transcription, chemotaxis, and other complex physiological processes. These regulatory systems consist of a sensor and regulatory protein, and, if any, signal transduction proteins that transmit the input signal sensed by the sensor protein to regulator proteins. Sensor proteins are the most upstream component in these regulatory systems, and the sensor and regulator proteins can be distinct molecules, or can sometimes exist in the same molecule as sensor and regulator domains. In both cases, the general scheme is as follows for biological regulatory systems by gas sensor proteins. Once a gas sensor protein/domain senses a gas molecule of its physiological effector, a conformational change of the sensor protein/domain is induced, and then intra- and/or inter-molecular signal transductions proceed to modulate the activity of the

regulator protein/domain that is responsible for the regulation of the above biological functions.

Elucidating the mechanisms of gas sensing and signal transduction is required to understand the structure and function of gas sensor proteins. To do this, the following questions should be answered. How do gas sensor proteins discriminate a physiological gas molecule from other gas molecules? What conformational changes are induced upon gas sensing, and how? How are the conformational changes induced by gas sensing related to the subsequent signal transduction process? How do intra- and inter-molecular signal transduction take place between the sensor and regulator protein/domain?

Gas sensor proteins that contain metal centers are advantageous for answering these questions, because the metal centers can serve as excellent spectroscopic probes in various applications such as UV/Vis, electron paramagnetic resonance (EPR), resonance Raman, circular dichroism (CD), and X-ray absorption spectroscopy (XAS). These methods can provide detailed information on the reactivity of the metal center with a gas molecule, and structural information around the metal center. X-ray crystallography is also an important tool to study gas sensor proteins. We have elucidated the structure and function relationships of the heme-based sensor proteins by these techniques.

Aer2 is a new MCP responsible for aerotaxis of *Pseudomonas aeruginosa*, which consists of N-terminal three-unit poly-HAMP, PAS, di-HAMP, and MCP domains. The Aer2 PAS domain contains a heme that acts as the active site for sensing O₂. Once the PAS domain senses O₂, intramolecular signal transduction will proceed from the PAS domain to the MCP domain. Though the HAMP domains are assumed to be responsible for intramolecular signal transduction, detail mechanisms remain to be elucidated.

We have determined the X-ray crystal structures of Aer2-N384 (residues 1-384 that consists of three-HAMP, PAS, and di-HAMP) and Aer2-PH (residues 173-384 that consists of PAS and di-HAMP) to elucidate the mechanism by which

intramolecular signal transduction proceeds between the HAMP and PAS domains in Aer2. Aer2-N384 is a homodimer having a non-crystallographic 2-fold symmetry as shown in Figure 1. The three-unit poly-HAMP, PAS, and di-HAMP domains are ordered in linear configuration. Most of the C-terminal di-HAMP domain is disordered.

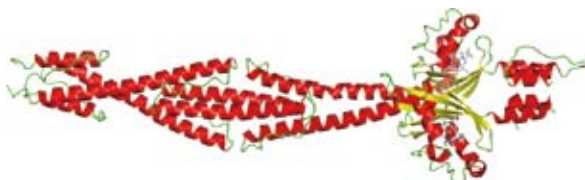


Figure 1. X-ray crystal structure of Aer2-N384 in cyano-met form.

Most of the di-HAMP domain is also disordered in the structure of Aer2-PH. A heme exists in a hydrophobic pocket in the PAS domain. His234 serves as the proximal ligand of the heme as shown in Figure 2. The 6-propionate forms a salt bridge with NE2 atom of His251, and the 7-propionate has hydrogen bonds with a water molecule, the main chain N atom of Lys235, and NE2 atom of Gln240. The heme-bound CN⁻ interacts with the side chain of Trp283. The distance is 2.9 Å between the N atom of CN⁻ and the NE2 atom of Trp283. CN-bound form of the heme can be thought to be a model of O₂-bound heme. The structure of Aer2-PH suggests that the heme-bound O₂ forms a hydrogen bond with Trp283. Trp283 is located on the C-terminal of the strand β5. This strand connects to the helix α5, which is the starting region of the C-terminal di-HAMP domain, suggesting that the hydrogen bond between Trp283 and O₂ are responsible for intramolecular signal transduction.

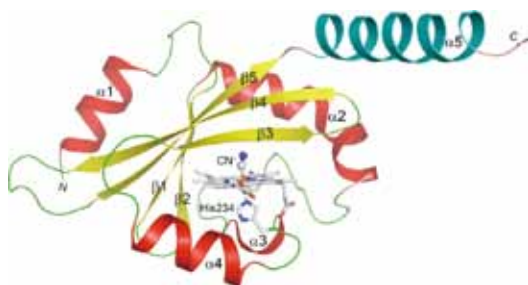


Figure 2. X-ray crystal structure of Aer2-PH in cyano-met form.

2. Structural Basis for the Transcriptional Regulation of Heme Homeostasis in *Lactococcus lactis*

Though a lactic acid bacterium *Lactococcus lactis* lacks

heme biosynthesis genes, it can uptake and use heme molecules provided externally to grow by oxygen respiration. As free heme molecules are toxic for cells, cellular concentrations of heme should be controlled strictly. *L. lactis* controls cellular heme concentrations by operating a heme efflux system. The expression of the heme efflux system is regulated by a heme-sensing transcriptional regulator HesR (heme efflux system regulator). In this work, we have determined X-ray crystal structures of HesR in heme-binding (holo-) and heme-free (apo-) forms to elucidate the structure and functions relationships of HesR.

HesR is a homo-dimer in the both of apo- and holo-forms as shown in Figure. HesR monomer consists of the N-terminal DNA-binding domain and the C-terminal heme binding domain that binds one heme molecule. Global fold of HesR is similar to that of TetR family transcriptional regulators. HesR is the first example of heme-sensing TetR family transcriptional regulator. A change in the relative orientation of the DNA-binding domain is induced upon heme-binding, which results in the regulation of DNA-binding activity of HesR.

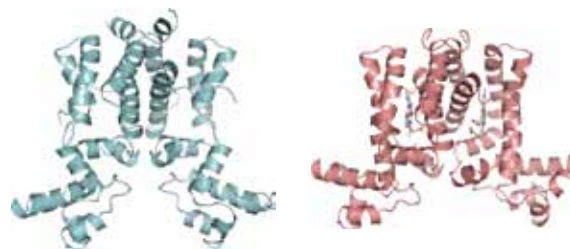


Figure 3. (Left) X-ray crystal structure of apo-HesR.

Figure 4. (Right) X-ray crystal structure of holo-HesR.

The HesR recognition sequence, ATGACACAGTGTCAT, is a perfect palindrome sequence as shown in the underlined sequence. We have found that apo-HesR can bind the target DNA, but holo-HesR can not. DNA-binding affinity of apo-HesR is determined to be $K_d = 0.7$ nM by fluorescence anisotropy measurements. These results indicate that heme molecule acts as a physiological effector of HesR to regulate its DNA-binding activity.

HesR shows a very high affinity for heme binding. When apo-HesR is mixed with holo-myoglobin, it can extract heme from myoglobin. The estimated heme binding affinity of HesR is comparable to that of myoglobin.

References

- 1) S. Aono, *Dalton Trans.* 3125–3248 (2008).
- 2) S. Aono, *Acc. Chem. Res.* **36**, 825–831 (2003).
- 3) S. Aono, *Antioxid. Redox Signaling* in press (2011).

Elucidation of the Molecular Mechanisms of Protein Folding

Department of Life and Coordination-Complex Molecular Science
Division of Biomolecular Functions



KUWAJIMA, Kunihiro
MAKABE, Koki
NAKAMURA, Takashi
CHEN, Jin
TAKENAKA, Toshio
MIZUKI, Hiroko
IKEDA, Yukako
TANAKA, Kei

Professor
Assistant Professor
IMS Research Assistant Professor
OIB Research Assistant Professor
Post-Doctoral Fellow
Technical Fellow
Technical Fellow
Secretary

Kuwajima group is studying mechanisms of *in vitro* protein folding and mechanisms of molecular chaperone function. Our goals are to elucidate the physical principles by which a protein organizes its specific native structure from the amino acid sequence. In this year, we studied the equilibrium and kinetics of bimolecular MgATP^{2-} binding to GroEL.

1. Dissecting a Bimolecular Process of MgATP^{2-} Binding to the Chaperonin GroEL

The chaperonin GroEL from *Escherichia coli*, a tetradecameric protein complex consisting of two heptameric rings stacked back to back with a central cavity, is one of the best characterized molecular chaperones that facilitate protein folding *in vivo*. The ATP^- dependent control of the affinity for its target protein and the co-chaperonin GroES is essential for its molecular chaperone function, and this control occurs through a series of cooperative allosteric transitions of GroEL induced by MgATP^{2-} . The equilibria and kinetics of the allosteric transitions of GroEL have thus been studied for some time by a variety of techniques. However, the initial bimolecular step of MgATP^{2-} binding to GroEL, which must precede the allosteric transitions, remains to be clarified.

Here, we studied the equilibrium and kinetics of MgATP^{2-} binding to a variant of GroEL, in which Tyr485 was replaced by tryptophan, via isothermal titration calorimetry (ITC) and stopped-flow fluorescence spectroscopy (Figures 1 and 2). In the absence of K^+ at 4 ~ 5 °C, the allosteric transitions and the subsequent ATP hydrolysis by GroEL are halted, and hence, the stopped-flow fluorescence kinetics induced by rapid mixing of MgATP^{2-} and the GroEL variant solely reflected MgATP^{2-} binding, which was well represented by bimolecular noncooperative binding with a binding rate constant, k_{on} , of $9.14 \times 10^4 \text{ M}^{-1} \text{ s}^{-1}$ and a dissociation rate constant, k_{off} , of 14.2 s^{-1} , yielding a binding constant, $K_{\text{b}} (= k_{\text{on}}/k_{\text{off}})$, of $6.4 \times 10^3 \text{ M}^{-1}$. We also successfully performed ITC to measure

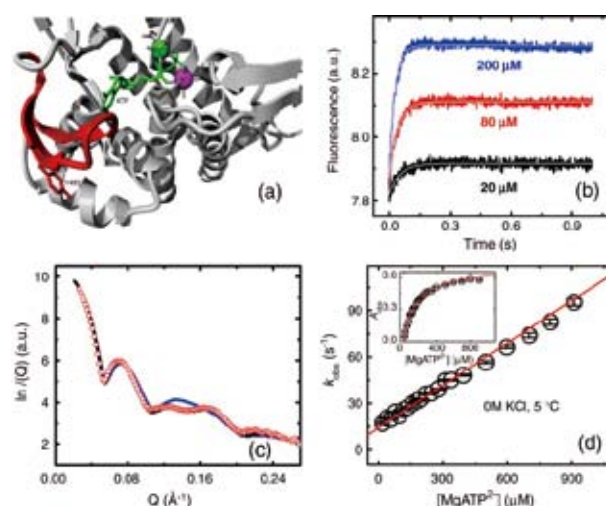


Figure 1. The structure around the MgATP^{2-} -binding site of GroEL (a), the SAXS patterns of wild-type GroEL in the different allosteric states (b), and the binding kinetics of MgATP^{2-} to GroEL(Y485W) (c and d).

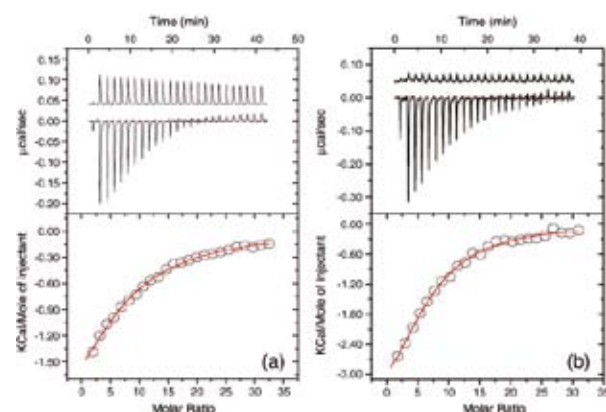


Figure 2. MgATP^{2-} -binding isotherms to GroEL(Y485W) (a) and GroEL(wild type) (b) measured by ITC in the absence of K^+ at 5 °C.

binding isotherms of MgATP^{2-} to GroEL and obtained a K_b of $9.5 \times 10^3 \text{ M}^{-1}$ and a binding stoichiometric number of 6.6 (Figure 2). K_b was thus in good agreement with that obtained by stopped-flow fluorescence. In the presence of 10 ~ 50 mM KCl, the fluorescence kinetics consisted of three to four phases (the first fluorescence-increasing phase, followed by one or two exponential fluorescence-decreasing phases, and the final slow fluorescence-increasing phase), and comparison of the kinetics in the absence and presence of K^+ clearly demonstrated that the first fluorescence-increasing phase corresponds to bimolecular MgATP^{2-} binding to GroEL. The temperature dependence of the kinetics indicated that MgATP^{2-} binding to GroEL was activation-controlled with an activation enthalpy

as large as 14 ~ 16 kcal mol⁻¹.

To further elucidate what kind of activation ($\text{P}^*\text{L} \rightarrow \text{PL}^\ddagger$) takes place during MgATP^{2-} binding to apo GroEL, we investigated the X-ray crystallographic structures of the MgATP^{2-} -binding site of apo GroEL (PDB code: 1OEL) and MgATP^{2-} -bound GroEL (PDB code: 1KP8). The MgATP^{2-} -bound GroEL, originally complexed with ATP γ S, assumed the T-state conformation, and hence provides an excellent model of the MgATP^{2-} -bound complex (PL) in the present study. As a result, the two structures were almost superimposable to each other. All atoms other than the O γ of Thr38 are not shifted more than 1.9 Å (Figure 3(a)).

If there is no essential difference in the binding-site structure between apo and MgATP^{2-} -bound GroEL, how can we explain the ΔH^\ddagger of 14 ~ 16 kcal mol⁻¹ that is involved in the activation step from P^*L to PL (Figure 3(b))? A possible explanation is given by partial dehydration and conformational strain in the transition-state complex (PL^\ddagger) that exists between P^*L and PL. Both MgATP^{2-} and the binding groove of GroEL are highly hydrated in P^*L , but these hydrated water molecules must be completely removed from the binding surface between MgATP^{2-} and the binding groove in PL, except for the two caves underneath the groove. In PL^\ddagger , MgATP^{2-} and the binding groove are thus only partially dehydrated, and this partial dehydration increases the energy level of PL^\ddagger as the final stabilization requires full dehydration. Furthermore, there may be conformational strain imposed on the binding groove in PL^\ddagger when specific interactions steer the ligand into the binding groove, and probably some openings at the entrance of the groove are required for accommodating MgATP^{2-} . Such conformational strain also increases the energy level of PL^\ddagger . As a result, the activation from P^*L to PL is accompanied by a ΔH^\ddagger as large as 14 ~ 16 kcal mol⁻¹. Interestingly, a very similar ΔH^\ddagger (16 kcal mol⁻¹) was observed in the reversed activation from P^*L to PL. In the reversed process, the partial hydration and the conformational strain similarly occur in PL^\ddagger , leading to the similar ΔH^\ddagger in the reversed activation process.

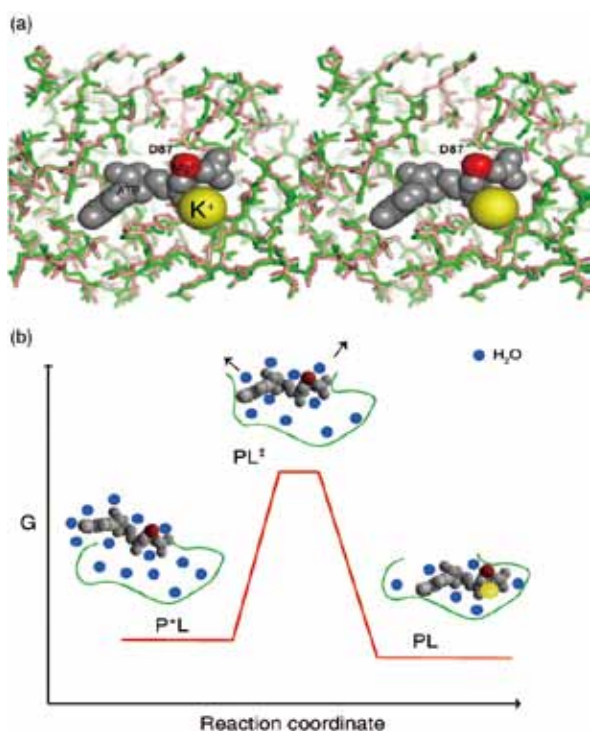


Figure 3. (a) A stereo view of superposition of X-ray structures of apo GroEL (green) (PDB code: 1OEL) and MgATP^{2-} -bound GroEL (pink) (PDB code: 1KP8) in a region around the binding site. (b) A reaction diagram of MgATP^{2-} binding to GroEL and schematic representations for the diffusional encounter complex (P^*L), the transition-state complex (PL^\ddagger), and the final stable complex (PL).

Reference

- 1) J. Chen, K. Makabe, T. Nakamura, T. Inobe and K. Kuwajima, *J. Mol. Biol.* **410**, 343–356 (2011).

Elucidation of Dynamical Structures of Biomolecules toward Understanding the Mechanisms Underlying Their Functions

Department of Life and Coordination-Complex Molecular Science
Division of Biomolecular Functions



KATO, Koichi
YAMAGUCHI, Takumi
KAMIYA, Yukiko
UEKUSA, Yoshinori
YAGI-UTSUMI, Maho
NGUYEN, Le Anh
TRINH XUAN, Anh
BOONSRI, Pornthip
BUI DINH, Long
SUGIHARA, Takahiro
CHANDAK, Mahesh
ZHANG, Ying
HIRANO, Takashi
UNO, Tsuyoshi
YAMAMOTO, Sayoko
SUZUKI, Mariko
ISONO, Yukiko
TANAKA, Kei

Professor
Assistant Professor
IMS Research Assistant Professor
Post-Doctoral Fellow
Post-Doctoral Fellow
Visiting Scientist
Visiting Scientist
Visiting Scientist
Visiting Scientist
Research Fellow
Graduate Student
Graduate Student
Graduate Student*
Graduate Student*
Graduate Student*
Technical Fellow
Technical Fellow
Secretary

Our biomolecular studies are based on detailed analyses of structures and dynamics of various biological macromolecules and their complexes at atomic level, primarily using NMR spectroscopy. Here we report NMR methods we recently developed for detailed conformational characterization of oligosaccharides and an NMR study of intermolecular interaction of amyloid β (A β) promoted on GM1 micelles.

1. Paramagnetic Lanthanide Tagging for NMR Conformational Analyses of *N*-Linked Oligosaccharides¹⁾

Although NMR spectroscopy has great potential to provide information on structure and dynamics of oligosaccharides, the applicability of the NOE-based approach, widely used for protein-structure determination, is limited by the insufficiency of distance-restraint information as a consequence of the low proton density in oligosaccharides and the exceedingly low number of proton-proton NOEs. Hence, to develop NOE-independent approaches for determining the oligosaccharide conformations and dynamics, we employed paramagnetic effects using novel lanthanide tags attached to the reducing end of an *N*-linked oligosaccharide.

Paramagnetic effects, such as pseudocontact shifts (PCSs) induced by lanthanide ions with an anisotropic magnetic susceptibility tensor, offer long-distance information on conformations and dynamics of biological macromolecules. For the development of a general method, we focused on the common core structure shared among all *N*-linked oligo-

saccharides, *i.e.* *N,N'*-diacetylchitobiose. An EDTA derivative designed to serve as the paramagnetic tag by chelating a lanthanide ion was attached to *N,N'*-diacetylchitobiose through amide linkage mimicking the '*N*-linked' oligosaccharides.

By ¹H-¹³C HSQC experiments using a series of paramagnetic lanthanide ions, the PCS values were measured as the differences of ¹H and ¹³C chemical shifts from those of the complex with the diamagnetic La³⁺ ion as a reference. For quantitative validation of our approach, the experimentally obtained PCS values were compared with those calculated from the 3D model of the complex based on a reported conformation of *N,N'*-diacetylchitobiose. The back-calculated PCS values are in excellent agreement with the experimental data demonstrating the utility of our approach. These results indicate that the common innermost part of the *N*-linked oligosaccharides exhibits a rigid conformation, which is little affected by the attachment of the tag (Figure 1). The conformational rigidity of the glycosidic linkage of this disaccharide agrees with results from molecular dynamics simulation. This success opens the door to conformational studies of a variety of sugar chains of biological interest.



Figure 1. 3D structural model of the lanthanide-tagged *N,N'*-diacetylchitobiose and its glycosidic torsional angles.

2. Development of Metabolic ^{13}C -Labeling Techniques for Carbohydrate NMR Analyses Using Genetically Engineered Yeast Strain²⁾

Applicability of NMR approach to carbohydrate conformational analyses will be strengthened by combining it with stable isotope labeling of the oligosaccharides. However, methodology of stable isotope labeling of sugar chains has been largely unexplored, especially for larger, branched oligosaccharides. In view of the situation, we developed a novel method for overexpression of homogeneous oligosaccharides with ^{13}C labeling using genetically engineered yeast strain.

We employed engineered *Saccharomyces cerevisiae* cells, in which a homogeneous high-mannose-type oligosaccharide accumulates because of deletions of genes encoding three enzymes involved in the processing pathway of *N*-linked oligosaccharides in the Golgi complex. Using uniformly ^{13}C -labeled glucose as the sole carbon source in the culture medium of these engineered yeast cells, high yields of the isotopically labeled $\text{Man}_8\text{GlcNAc}_2$ (M8B) oligosaccharide could be successfully harvested from glycoprotein extracts of the cells. This enabled to observe ^1H - ^{13}C HSQC spectrum at a proton observation frequency of 920.7 MHz. Furthermore, ^{13}C labeling at selected positions of the sugar residues in the oligosaccharide could be achieved using a site-specific ^{13}C -enriched glucose as the metabolic precursor, facilitating NMR spectral assignments (Figure 2). The ^{13}C -labeling method thus established provides the technical basis for NMR analyses of structures, dynamics, and interactions of larger, branched oligosaccharides.

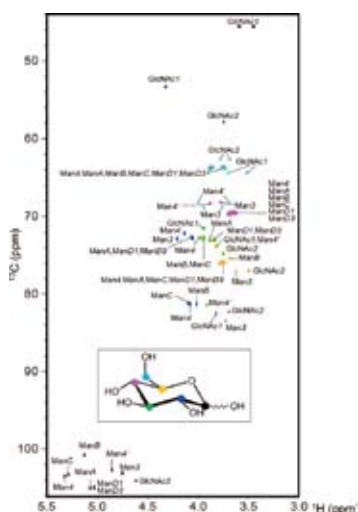


Figure 2. ^1H - ^{13}C HSQC spectra of the pyridylamino derivative of M8B, metabolically ^{13}C -labeled using site-specific ^{13}C -enriched glucose isotopomers.

Award

KATO, Koichi; The Pharmaceutical Society of Japan Award for Divisional Scientific Promotions.

YAGI-UTSUMI, Maho; The Protein Science Society of Japan Incentive Award for Young Investigators, The 11th Annual Meeting of the Protein Science Society of Japan (2011).

3. Spectroscopic Characterization of Intermolecular Interaction of Amyloid β Promoted on GM1 Micelles³⁾

Clusters of GM1 gangliosides act as platforms for conformational transition of monomeric, unstructured A β to its toxic β -structured aggregates. We previously reported that A β (1-40) is accommodated on the hydrophobic/hydrophilic interface of the ganglioside cluster exhibiting an α -helical conformation under ganglioside-excess conditions. To gain further insights into the underlying mechanisms of the amyloid formation of A β , it is necessary to characterize the conformational transition from α -helices to β -structures of A β on the ganglioside clusters.

We characterized conformational states of A β (1-40) in the presence of varying amounts of GM1 aqueous micelles using stable-isotope-assisted NMR spectroscopy in conjunction with synchrotron-radiation vacuum-ultraviolet CD spectroscopy. We found that GM1 micelles induce distinct secondary structures of A β (1-40) depending on the A β /GM1 ratios. Furthermore, it was revealed that the thioflavin T (ThT)-reactive β -structure is more populated in A β (1-40) under conditions where the A β (1-40) density on GM1 micelles is high. Under this circumstance, the C-terminal hydrophobic anchor Val39-Val40 shows two distinct conformational states that are reactive with ThT, while such A β species were not generated by smaller lyso-GM1 micelles (Figure 3). These findings suggest that GM1 clusters promote specific A β -A β interactions through their C-termini coupled with formation of the ThT-reactive β -structure depending on sizes and curvatures of the clusters.

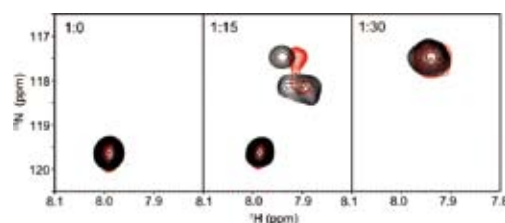


Figure 3. ^1H - ^{15}N HSQC peak originating from Val39 of A β (1-40) titrated with GM1 micelles in the presence or absence of ThT. The spectra measured in the absence (black) and presence (red) of ThT are overlaid.

References

- 1) S. Yamamoto, T. Yamaguchi, M. Erdélyi, C. Griesinger and K. Kato, *Chem. -Eur. J.* **17**, 9280–9282 (2011).
- 2) Y. Kamiya, S. Yamamoto, Y. Chiba, Y. Jigami and K. Kato, *J. Biomol. NMR* **50**, 397–401 (2011).
- 3) M. Yagi-Utsumi, K. Matsuo, K. Yanagisawa, K. Gekko and K. Kato, *Int. J. Alzheimers. Dis.* **2011**, 925073 (8 pages) (2011).

* carrying out graduate research on Cooperative Education Program of IMS with Nagoya City University

Structure-Function Relationship of Metalloproteins

Department of Life and Coordination-Complex Molecular Science
Division of Biomolecular Functions



FUJII, Hiroshi
KURAHASHI, Takuya
CONG, Zhiqi
OHTSUKI, Akimichi
WANG, Chunlan
TANIZAWA, Misako

Associate Professor
Assistant Professor
IMS Fellow
Post-Doctoral Fellow
Graduate Student
Secretary

Metalloproteins are a class of biologically important macromolecules, which have various functions such as oxygen transport, electron transfer, oxidation, and oxygenation. These diverse functions of metalloproteins have been thought to depend on the ligands from amino acid, coordination structures, and protein structures in immediate vicinity of metal ions. In this project, we are studying the relationship between the electronic structures of the metal active sites and reactivity of metalloproteins.

1. One-Electron Oxidation of Electronically-Diverse Manganese(III) and Nickel(II) Salen Complexes: Transition from Localized to Delocalized Mixed-Valence Ligand Radicals¹⁾

Ligand radicals from salen complexes are unique mixed-valence compounds, in which a phenoxyl radical is electronically linked to a remote phenolate via a neighboring redox-active metal ion, providing an opportunity to study electron transfer from a phenolate to a phenoxyl radical mediated by a redox-active metal ion as a bridge. We herein synthesize one-electron oxidized products from electronically-diverse manganese(III) salen complexes, in which the locus of oxidation is shown to be ligand-centered, not metal-centered, affording manganese(III)–phenoxyl radical species. The key point in the present study is an unambiguous assignment of IVCT (intervalence charge transfer) bands by using non-symmetrical salen complexes, which enables us to obtain otherwise inaccessible insight into the mixed-valence property.

A d^4 high-spin manganese(III) ion forms a Robin-Day Class II mixed-valence system, in which electron transfer is occurring between the *localized* phenoxyl radical and the phenolate. This is in clear contrast to a d^8 low-spin nickel(II) ion with the same salen ligand, which induces a *delocalized* radical (Robin-Day Class III) over the two phenolate rings, as previously reported by others. The present findings point to a fascinating possibility that electron transfer could be drastically modulated by exchanging the metal ion that bridges the two redox centers.

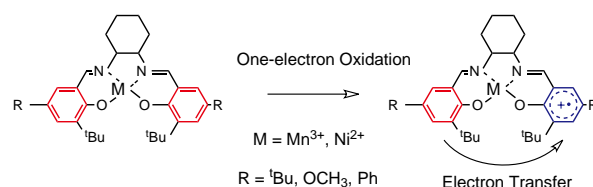


Figure 1. Mixed-Valence Ligand Radicals formed from manganese (III) and nickel(II) salen Complexes.

2. Redox Potentials of Oxoiron(IV) Porphyrin π -Cation Radical Complexes: Participation of Electron Transfer Process in Oxygenation Reactions²⁾

The oxoiron(IV) porphyrin π -cation radical complex (compound I) has been identified as the key reactive intermediate of several heme enzymes and synthetic heme complexes. The redox properties of this reactive species are not yet well understood. Here, we report the results of a systematic study

of the electrochemistry of oxoiron(IV) porphyrin π -cation radical complexes with various porphyrin structures and axial ligands in organic solvents at low temperatures. The cyclic voltammogram of (TMP)Fe^{IV}O, (TMP = 5,10,15,20-tetramesitylporphyrinate), exhibits two quasi-reversible redox waves at $E_{1/2} = 0.88$ and 1.18 V vs. SCE in dichloromethane at -60 °C (Figure 2). Absorption spectral measurements for electrochemical oxidation at controlled potential clearly indicated that the first redox wave results from the (TMP)Fe^{IV}O/[(TMP⁺)Fe^{IV}O]⁺ couple. The redox potential for the (TMP)Fe^{IV}O/[(TMP⁺)Fe^{IV}O]⁺ couple undergoes a positive shift upon coordination of an anionic axial ligand, but a negative shift upon coordination of a neutral axial ligand (imidazole). The negative shifts of the redox potential for the imidazole complexes are contrary to their high oxygenation activity. On the other hand, the electron-withdrawing effect of the meso-substituent shifts the redox potential in a positive direction. Comparison of the measured redox potentials and reaction rate constants for epoxidation of cyclooctene and demethylation of *N,N*-dimethylanilines enable us to discuss the details of the electron transfer process from substrates to the oxoiron(IV) porphyrin π -cation radical complex in the oxygenation mechanisms.

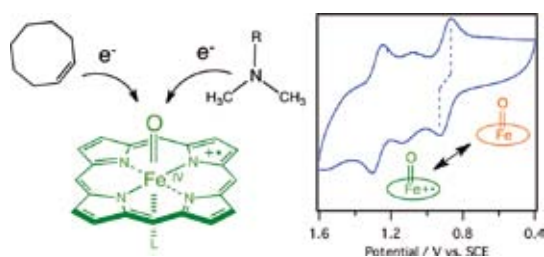


Figure 2. Cyclic Voltammogram of Oxoiron(IV) Porphyrin π -Cation Radical Complex.

3. Oxidation of Chloride Ion and Subsequent Chlorination of Organic Compounds by Oxoiron(IV) Porphyrin π -Cation Radical Complexes³⁾

Chloroperoxidase (CPO) and myeloperoxidase (MPO) are the only heme peroxidases that catalyze oxidation of chloride ion with hydrogen peroxide. CPO is an enzyme of *Caldariomyces fumago* and catalyzes chlorination reactions in the biosynthesis of chlorine-containing compounds. CPO is also known to exhibit peroxidase, catalase, and cytochrome P450-like activities. CPO has a thiolate heme axial ligand like cytochrome P450. This makes CPO distinct from other heme

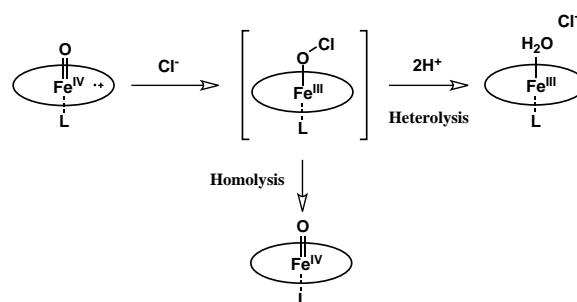


Figure 3. Cyclic Voltammogram of Oxoiron(IV) Porphyrin π -Cation Radical Complex.

peroxidases which have a histidine imidazole as the heme axial ligand. On the other hand, MPO is found in the granules of myelocytes (precursors of neutrophils), and works as a major component of the antimicrobial system of neutrophils. MPO belongs to the animal peroxidase superfamily and has an imidazole heme axial ligand. Numerous biological studies have suggested that an oxoiron(IV) porphyrin π -cation radical species known as compound I, is responsible for oxidation of chloride ion and for addition of a chloride ion to the ferryl oxygen atom of compound I to produce a transient ferric hypochlorite complex, Fe(III)-OCl. The ferric hypochlorite complex is believed to act as a key compound in the reactions leading to chlorination of organic substrates by CPO and antimicrobial activity in MPO. Although the oxidation process has been studied by multi-mixing stopped-flow experiments in which transiently formed compound I were reacted with chloride ion, spectroscopic evidence for the formation of the ferric hypochlorite complex has not been obtained and it remains unclear how compound I oxidizes chloride ion. Furthermore, the identity of the true chlorinating agent in the subsequent chlorination of organic substrates is not known and more information is needed about the exact roles of the hypochlorite adduct, free hypochlorous acid, and Cl₂. Here, we report the direct observation of oxidation of chloride ion with synthetic compound I model complexes and subsequent reactions leading to chlorination of organic compounds (Figure 3).

References

- 1) T. Kurahashi and H. Fujii, *J. Am. Chem. Soc.* **133**, 8307–8316 (2011).
- 2) A. Takahashi, T. Kurahashi and H. Fujii, *Inorg. Chem.* **49**, 6922–6928 (2011).
- 3) Z. Cong, T. Kurahashi and H. Fujii, *Angew. Chem., Int. Ed.* **50**, 9935–9939 (2011).

Fabrication of Silicon-Based Planar Ion-Channel Biosensors and Integration of Functional Cell Membrane Model Systems on Solid Substrates

Department of Life and Coordination-Complex Molecular Science
Division of Biomolecular Sensing



URISU, Tsuneo
TERO, Ryugo
WANG, Zhihong
RAHMAN, Mashiur
ASANO, Toshifumi
NAGAIRO, Takeshi
NAGAOKA, Yasutaka
UNO, Hidetaka
NAKAI, Naohito
SHANG, Zhi-Guo
FUJIWARA, Kuniyo
SHIMIZU, Atsuko

Professor*
Assistant Professor†
Post-Doctoral Fellow
Post-Doctoral Fellow
Post-Doctoral Fellow
Post-Doctoral Fellow
Research Fellow
Graduate Student
Graduate Student
Graduate Student
Graduate Student
Secretary

We are interested in the investigation of cell membrane surface reactions and the pathogen mechanism of the neuro-degenerative diseases, based on the molecular science. We are advancing two subjects, aiming the creation and development of new molecular science field, “medical molecular science.” One is the development of ion channel biosensor and its application to the neural network analyzer device. The other is the fundamental understanding of bilayer membrane properties using the artificial lipid bilayers on solid substrates, which is called supported bilayers, by means of atomic force microscope and fluorescence microscope-based techniques.

1. Development of Neural Network Device and Precise Microfabrications

Although the patch-clamp method using the pipette is now in practical use, it is not suitable for miniaturization and high throughput screening applications, since the measurement system is large and requires high level of skills for operations. It is expected that the breakthrough for these technical problems can be realized by the planarization of the device. For the planar typed ion channel biosensor, glass (Fertig, 2002), Si (Sordel, 2006, Matthews, 2006, Pantoja, 2004), quartz (Sett, 2003) and a silicon elastomer PDMS (Li, 2006), *etc.* have been reported as the substrate materials. And for Si, it has been considered that the background noise current is large due

to the free charge carrier density in the substrate. However, we have recently demonstrated that the noise current can be significantly reduced by using silicon-on-insulator (SOI) or polymethyl methacrylate (PMMA) substrate.

Commercialized planar patch clamp devices, however, can not be used in a system that requires long incubation periods. New functional analysis and/or screening devices could be realized by adding an incubation function to the planar patch clamp method, and these would be especially useful in applications such as *in vitro* systems of neurons and neural networks using dissociated cultured neurons (Tao, 2000, Taylor, 2010, Reska, 2008, Erickson, 2008). Moreover, the planar patch clamp method enables simultaneous measurement of multi-point ion channel currents and advanced 2-D bio-imaging. We have developed an incubation type of planar patch clamp device and demonstrated its operation using TRPV1-expressing HEK293 cells and capsaicin as a ligand molecule. Detailed investigation about the basic properties have not yet been done.

The recently developed light-gated ion-channel method is extremely suitable for the investigation of neural cell and/or neural network functional analysis due to its excellent time and space resolutions (Petreanu, 2007). Concerning the application of light-gated ion-channel in the planar patch clamp method, however, no investigation has been done, in spite of its extreme importance.

In this work, ion channel biosensor based on the incu-

bation type planar patch clamp method was developed and the basic properties were investigated. Due to the existence of ECM protein at the cleft between the cell membrane and the substrate surface near the micropore, it is not easy to realize the high seal resistance (giga-ohm seal). In the present case using collagen 4 as ECM, the seal resistance was usually about 10 M Ω , and the noise level was 7 pA with the 1 kHz low pass filter (Figure 1). The main noise sources were excess current noise and the thermal noise generated at micro pore resistance (R_a) and the seal resistance (R_j). All these noises can be reduced by increasing the seal resistance. Operation of the

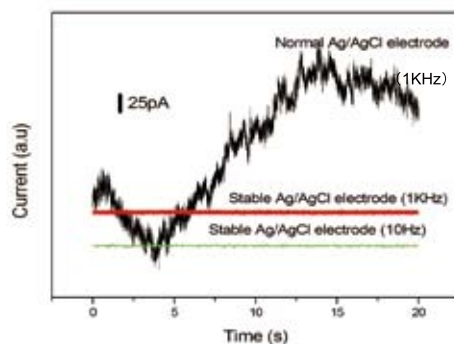


Figure 1. Observed current noise in the biosensor system.

light-gated ion channel, ChRWR, was investigated by the incubation type planar patch clamp method using laser ($\lambda = 473$ nm) stimulations (Figure 2). The channel current profile and its membrane potential dependence well agreed to the

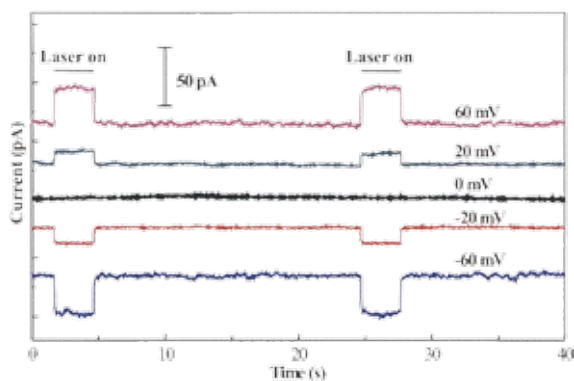


Figure 2. Observed ion channel current under voltage clamp of 473-nm laser irradiation with ChRWR-expressing HEK293. Ion channel current wave forms depend on the applied membrane potentials.

reported data measured by pipette patch clamp method. So we think that light-gated method is also useful in the neural network function analysis and high throughput screening application based on the incubation type planar patch clamp method, and also useful in the simple performance check of these devices. The biosensor operation was examined, using TRPV1-expressing HEK293 cells. Quite high sensitivity was confirmed. But for the single channel recordings, several times improvement of the seal resistance is required.

2. Extracellular Matrix Patterning for Cell Alignment by Atmospheric Pressure Plasma

Low-temperature atmospheric-pressure plasma (APP) jets and a metal stencil mask have been used for the patterning of fibronectins deposited on a silicon (Si) wafer. Fibronectins typically constitute the extracellular matrix (ECM) and a micro-patterned ECM may be used for arranging living cells in a desired pattern on the substrate surface. Such a technique can be used for the fabrication of cell chips. In this study, patterning of 100 nm wide lines of fibronectin layers has been demonstrated. Desorption of fibronectins from the surface by plasma application has been confirmed by atomic force microscopy (AFM) (Figure 3), and Fourier transform infrared spectroscopy (FT-IR).

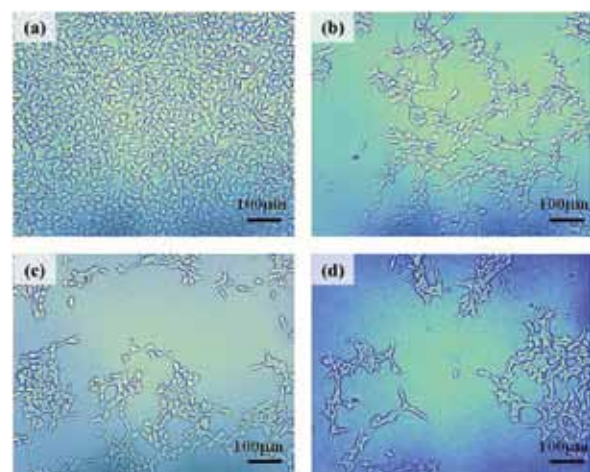


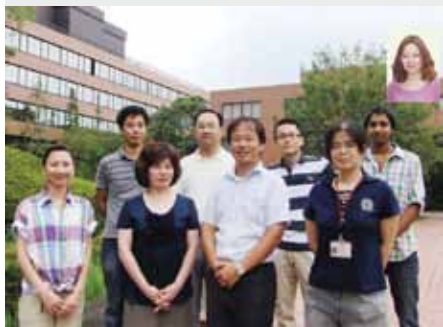
Figure 3. Photomicrographs of the sample substrate surface after plasma application of (a) 0 s (b) 10 s, (c) 20 s and (d) 30 s. The photographs were taken after 72 hours cell cultivation.

* Present Address: Nagoya University

† Present Address: Electronics-Inspired Interdisciplinary Research Institute, Toyohashi University of Technology

Investigation of Molecular Mechanisms of Transporters and Receptors in Membrane

Department of Life and Coordination-Complex Molecular Science
Division of Biomolecular Sensing



FURUTANI, Yuji	Associate Professor
KIMURA, Tetsunari	Assistant Professor
TSUKAMOTO, Hisao	IMS Research Assistant Professor
MEENA, Yatindra Shingh	Visiting Scientist
GUO, Hao	Graduate Student
FUJIWARA, Kuniyo	Graduate Student
INAGUMA, Asumi	Graduate Student
MURAMATSU, Chikako	Graduate Student*
SHIMIZU, Atsuko	Secretary

Membrane proteins are important for homeostasis of living cells, which work as ion channel, ion pump, various types of chemical and biophysical sensors, and so on. These proteins are considered as important targets for biophysical studies. However, their molecular mechanisms have not been studied well, because X-ray crystallography and NMR spectroscopy are hard to access them in general.

Our main goal is to clarify molecular mechanisms of transporters and receptors in cell membrane mainly by using stimulus-induced difference infrared (IR) spectroscopy, which is sensitive to the structural and environmental changes of organic and bio- molecules. In this year, Dr. Kimura has started to construct a microfluidic device to monitor biological and chemical reactions by infrared and fluorescent microscopic techniques.

1. Perfusion-Induced Difference FT-IR Spectroscopy for Na⁺-Pump V-ATPase

Attenuated total reflection (ATR) FT-IR spectroscopy is a powerful technique to obtain infrared spectra of membrane proteins immersed in aqueous solution.^{1,2)} By exchanging buffer with and without salts, the difference spectra between the two conditions provide the structural information relating to the interaction between protein and ions. In this year, application of this technique to a transporter protein (V-ATPase) has been published in JACS.

V-ATPase from *Enterococcus hirae*, which forms a large supramolecular protein complex (total molecular weight: ~700,000), physiologically transports Na⁺ and Li⁺ across a hydrophobic lipid bilayer. Stabilization of these cations in the binding site has been discussed based on the X-ray crystal structures of a membrane-embedded domain, named the K-ring (Na⁺ and Li⁺ bound forms). Here, we applied ATR-FTIR spectroscopy on this large protein complex for the first time, and we measured sodium or lithium ion binding-induced difference infrared spectra of the intact V-ATPase with sufficient amount of hydration at physiological temperature.¹⁾ The results suggest that binding of sodium or lithium ion induces

the deprotonation of Glu139, resulting in a hydrogen-bonding change around a tyrosine residue and a little conformational change in the K-ring. These structural changes, especially the deprotonation of Glu139, are considered to be important for reducing energetic barriers to the transport of the cations across membranes.

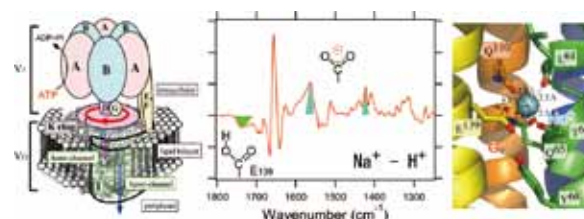


Figure 1. (left) Schematic structure of whole V-ATPase protein complex (center) Sodium ion binding induced difference infrared spectrum. The green and cyan colored bands are assigned to protonated and deprotonated carboxylic acid residues of Glu139 in K-ring, respectively. (right) Sodium ion binding site revealed by X-ray crystallography on K-ring.

2. Ion-Selective Mechanism of Mg²⁺ Transporter MgtE Studied by ATR FT-IR

Mg²⁺ is the most abundant divalent cation in living cells. MgtE is one of the Mg²⁺ transporters that function in the homeostasis of the intracellular Mg²⁺ concentration, in which the cytosolic domain acts as a ‘Mg²⁺ sensor’ and the transmembrane (TM) domain works as a ‘pore.’ Under high-intracellular Mg²⁺ conditions (> 10 mM), Mg²⁺ binding to the MgtE stabilizes a “closed” state and shuts down the Mg²⁺ transport from the extracellular part. In contrast, under low-intracellular Mg²⁺ conditions (< 1 mM), the MgtE is in equilibrium between the “closed” and “open” states, which can transport Mg²⁺. In addition, MgtE is a highly Mg²⁺-selective channel and unable to transport other divalent-cations including near-cognate Ca²⁺. We performed the perfusion-induced difference ATR-FTIR measurements to understand the molecular mechanism underlying the Mg²⁺-selectivity of MgtE.

The difference FTIR spectrum between the magnesium- and calcium-binding forms showed the bands between 1430 and 1380 cm^{-1} which are assigned to carboxylate groups. The COO^- bands in the presence of Mg^{2+} were observed in the higher wavenumber than in the presence of Ca^{2+} , indicating weaker interaction of the carboxylate groups with Mg^{2+} than with Ca^{2+} . This result contradicts the stronger electrostatic interaction of fully hydrated Mg^{2+} with COO^- group compared with Ca^{2+} . On the other hand, the titration experiment for the closed states revealed that there are some binding sites to which Mg^{2+} binds ~ 40 times higher affinity than Ca^{2+} binds. The Mg^{2+} -binding site composed of the Asp432 in the TM domain (Mg1 site) is a plausible candidate based on our mutagenesis and protease protection experiments. These results suggest that the higher affinity for Mg^{2+} is due to the size of the cavity that can accommodate the hydrated Mg^{2+} rather than its charge intensity.

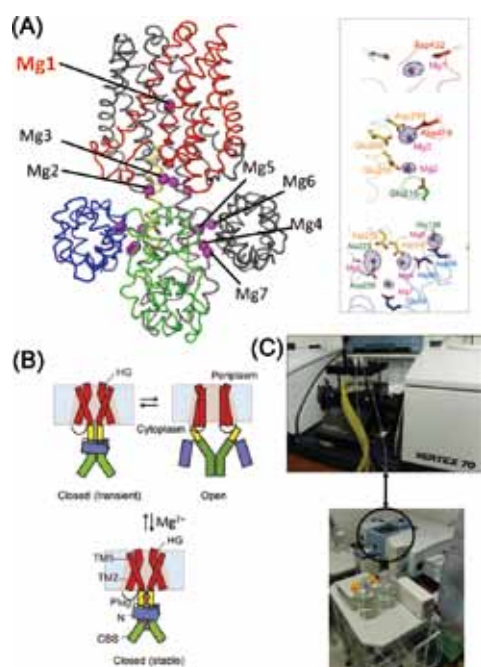


Figure 2. (A) X-ray crystal structure of MgtE in the closed state. *Inset:* Divalent cation binding sites. (B) Proposed gating mechanism of MgtE. (C) Pictures of the perfusion-induced difference ATR-FTIR measurements system.

3. Surface Enhanced Infrared Spectroscopy for Membrane Proteins in a Single Sheet of Lipid Bilayers

Monitoring structural changes of membrane proteins in a

Award

GUO, Hao; FY2011 (the 2nd) Sokendai President's Award.

single sheet of lipid bilayer has been considered to be an ideal measurement method, while it is probably hard to detect tiny spectral change of the single-layered proteins. A graduate student, Mr. Hao Guo, has been struggling to establish the method. He got an award from SOKENDAI in advance of publication. In the near future, we will accomplish this challenging subject.

4. Development of a Microfluidic Device to Monitor Biological and Chemical Reactions

Real-time observation is one of the powerful techniques to understand the molecular mechanisms of the self-organization and molecular association. The solution mixing technique realizes many reaction fields for biological and chemical reactions by changing the buffer condition and can be combined with spectroscopic equipment easily. However, conventional mixing techniques limit their targets because of the large consumption of the sample. We are developing a novel microfluidic device and trying to reduce the sample consumption to $\sim 1/1000$. In addition, we aim to achieve the time-resolution of several microseconds by combining with microscopic techniques.

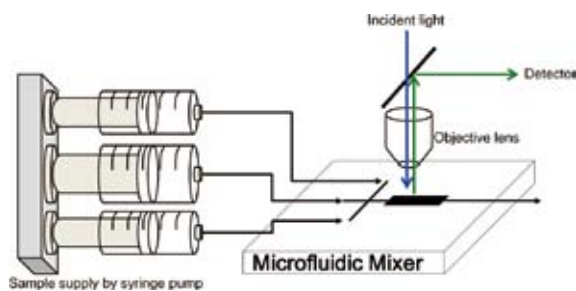


Figure 3. Schematic drawing of the microfluidic mixer.

Acknowledgements

We thank many collaborators, especially Prof. Hideki Kandori (Nagoya Institute of Technology) and Assoc. Prof. Takeshi Murata (Chiba University) for V-ATPase project, Prof. Osamu Nureki and Assoc. Prof. Ryuichiro Ishitani (University of Tokyo) for MgtE project.

References

- 1) Y. Furutani, T. Murata and H. Kandori, *J. Am. Chem. Soc.* **133**, 2860–2863 (2011).
- 2) J. Sasaki, H. Takahashi, Y. Furutani, H. Kandori and J. L. Spudich, *Biophys. J.* **100**, 2178–2183 (2011).

Heterogeneous Catalytic Systems for Organic Chemical Transformations in Water

Department of Life and Coordination-Complex Molecular Science
Division of Complex Catalysis



UOZUMI, Yasuhiro
OSAKO, Takao
HAMASAKA, Go
ZHOU, Haifeng
KOBAYASHI, Noboru
MUTO, Tsubasa
SAKURAI, Fumie
TORII, Kaoru
TAZAWA, Aya
SASAKI, Tokiyo
FUKUSHIMA, Tomoko

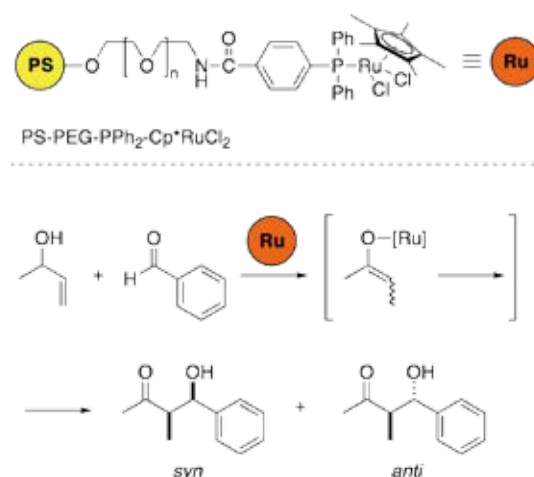
Professor
Assistant Professor
Post-Doctoral Fellow
Post-Doctoral Fellow
Graduate Student
Graduate Student
Graduate Student
Technical Fellow
Technical Fellow
Secretary
Secretary

Various transition metal-catalyzed organic molecular transformations in water were achieved under heterogeneous conditions by use of an amphiphilic resin-supported ruthenium complexes, a boron-iridium heterobimetallic polymeric catalyst, or an architecture-based system of transition metal catalysis using an amphiphilic pincer palladium complex bearing hydrophilic and hydrophobic chains which were designed and prepared by this research group. In particular, tandem olefin migration-aldol condensation and dehydrative alkylation, which were performed in water under heterogeneous conditions, and development of an amphiphilic pincer palladium complex bearing hydrophilic and hydrophobic chains for an architecture-based system of transition metal catalysis are highlights among the achievements of the 2010–2011 period to approach what may be considered ideal chemical processes of next generation. Representative results are summarized hereunder.

1. Tandem Olefin Migration-Aldol Condensation in Water with an Amphiphilic Resin-Supported Ruthenium Complex^{1,2)}

A catalytic tandem olefin migration/aldol condensation process with allylic carbinols and aryl aldehydes was performed with an amphiphilic polystyrene-poly(ethylene glycol) (PS-PEG) resin-supported phosphine-ruthenium complex in water as a single reaction medium under heterogeneous conditions. It is noteworthy that the catalytic performance of the polymeric complex PS-PEG-phosphine-RuCl₂Cp* in water was much higher than that reported for ruthenium-phosphine complexes (e.g. RuCl₂(PPh₃)₃) under homogeneous conditions. Thus, 0.5 mol% Ru of the polymeric catalyst promoted the tandem olefin migration/aldol condensation in water at 45

°C within 2 h to give quantitative yields of the corresponding aldols with *syn*-selectivity. Inverse stereoselectivity (*anti*-selectivity) was observed when the reaction was carried out in the presence of K₂CO₃.

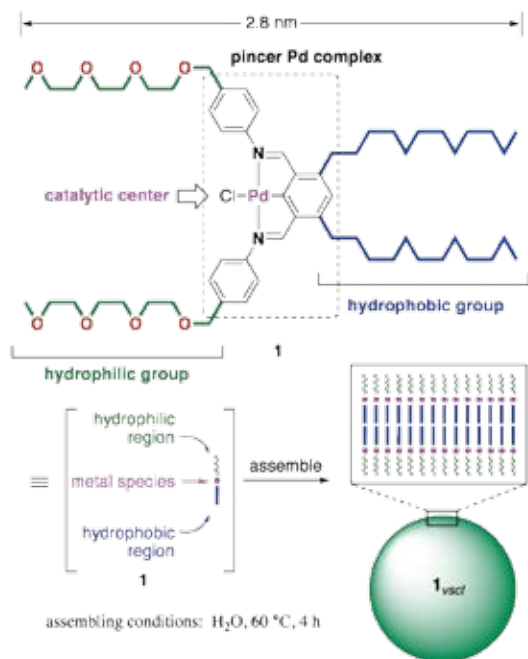


Scheme 1. Tandem Olefin Migration-Aldol Condensation in Water with Amphiphilic Resin-Supported Ruthenium Complex.

2. Molecular Architecture-Based Administration of Catalysis in Water via Self-Assembly of an Amphiphilic Palladium Pincer Complex³⁾

An architecture-based system of transition metal catalysis using an amphiphilic pincer palladium complex bearing hydrophilic and hydrophobic chains was developed, where (i) the self-assembling formation of bilayer vesicles of a palladium complex, (ii) the concentration of organic substrates at the

hydrophobic region of the bilayer membrane, (iii) and the catalytic transformation of the substrate with the palladium species, all located in a close diffusion distance, automatically occurred in water. The oxirane ring opening reaction and the Michael reaction, both with arylboron reagents, were found to proceed in water where the vesicle structure of the palladium complex was essential to promote catalysis.

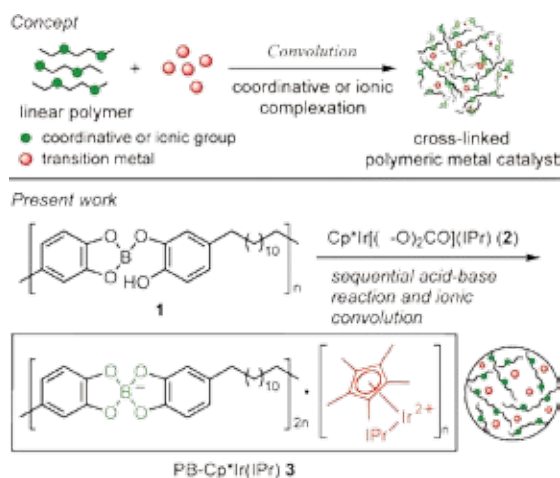


Scheme 2. Formation of Vesicle **1_{vsc1}** by Self-Assembly of the Pincer Palladium Complex **1** (top) and Schematic Image of the Concept of Catalysis within the Bilayer membrane of the **1_{vsc1}** (bottom).

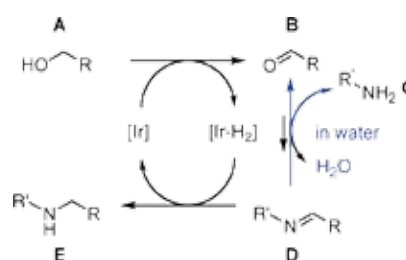
3. In-Water Dehydrative Alkylation of Ammonia and Amines with Alcohols by a Polymeric Bimetallic Catalyst⁴

We have previously developed new methodology for the preparation of highly active and reusable polymer-supported catalysts, also known as “molecular convolution,” where a soluble linear polymer having multiple ligand groups was convoluted with neutral metals or anionic metal salts via

coordinative or ionic complexation to achieve the one-step preparation of the insoluble polymeric metal composite, combining heterogeneity and catalytic activity in one system. A novel convoluted polymeric metal catalyst was designed and prepared for the first time to realize “in-water dehydrative *N*-alkylation.” Thus, a boron-iridium heterobimetallic polymeric catalyst was prepared by ionic convolution of a poly (catechol borate) and an iridium complex. The alkylation of ammonia and amines with alcohols, alkylating agents, was performed with 1 mol% Ir of the heterogeneous catalyst in water without the use of organic solvents under aerobic conditions to give the corresponding alkylated amines in up to quantitative yield.



Scheme 3. Concept for the Molecular Convolution (top) and Preparation of PB-Cp*Ir(Ir) (bottom).



Scheme 4. Proposed Mechanism for In-Water Dehydrative *N*-Alkylation with PB-Cp*Ir(Ir).

References

- 1) Y. Oe and Y. Uozumi, *Adv. Synth. Catal.* **350**, 1771–1775 (2008).
- 2) Y. Oe and Y. Uozumi, *Synlett* 787–790 (2010).
- 3) G. Hamasaka, T. Muto and Y. Uozumi, *Angew. Chem., Int. Ed.* **50**, 4876–4878 (2011).
- 4) H. Ohta, Y. Yuyama, Y. Uozumi and Y. M. A. Yamada, *Org. Lett.* **13**, 3892–3895 (2011).

Synthesis of Metal Complexes Aiming at Storage and Release of Chemical Energy

Department of Life and Coordination-Complex Molecular Science
Division of Functional Coordination Chemistry



TANAKA, Koji	Professor
OHTSU, Hideki	Assistant Professor
KOBAYASHI, Katsuaki	IMS Research Assistant Professor
PADHI, Sumanta Kumar	Post-Doctoral Fellow
NAKANE, Daisuke	Post-Doctoral Fellow
YAMAGUCHI, Yumiko	Secretary
NOGAWA, Kyoko	Secretary

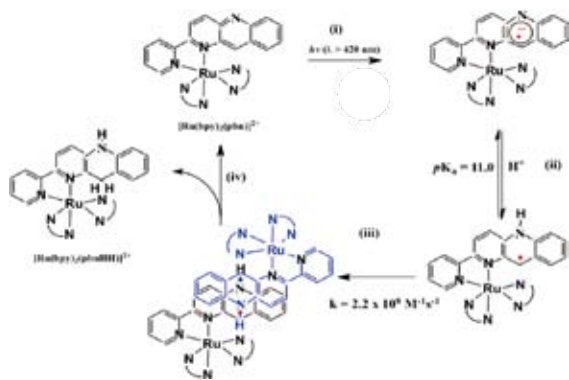
Artificial photosynthetic processes aimed at carbon dioxide reduction and water splitting are top research priorities for coping with the energy shortage that is anticipated in the near future to result from depletion of fossil fuels. Photoinduced one-electron transfer inevitably generates high-energy free radical intermediates that often trigger undesired side reactions, which is a serious issue that remains to be overcome. Proton coupled electron transfer is expected to substantially stabilize such radical intermediates, and could play a key role in multi-electron transfer to the relevant reaction sites involved in carbon dioxide reduction and water splitting.

Recently, we found that mono-nuclear $[\text{Ru}(\text{bpy})_2(\text{pbn})](\text{PF}_6)_2$ ($[\mathbf{1}]^{2+}$; bpy = 2,2'-bipyridine, pbn = 2-(2-pyridyl)-benzo[*b*]-1,5-naphthyridine) is smoothly reduced to $[\text{Ru}(\text{bpy})_2(\text{pbnH}_2)](\text{PF}_6)_2$ ($[\mathbf{1}\cdot\text{H}_2]^{2+}$; pbnH₂ = 5,10-dihydro-2-(2-pyridyl)benzo[*b*]-1,5-naphthyridine) by photoinduced two-electron reduction of pbn under irradiation with visible light in the presence of a sacrificial reagent. The reaction mechanism for the photoassisted two-electron reduction of $[\mathbf{1}]^{2+}$ (Scheme 1) is explained as follows; i) photoexcitation of $[\mathbf{1}]^{2+}$ and the subsequent reductive quenching of the photoexcited $[\mathbf{1}]^{2+*}$ by

a sacrificial donor produces $[\text{Ru}(\text{bpy})_2(\text{pbn}^{\bullet-})]^+$ ($[\mathbf{1}]^+$), ii) protonation of the non-coordinating nitrogen of the pbn^{•-} of $[\mathbf{1}]^+$ generates $[\text{Ru}(\text{bpy})_2(\text{pbnH}^{\bullet})]^{2+}$ ($[\mathbf{1}\cdot\text{H}]^{2+}$), iii) rapid dimerization of $[\mathbf{1}\cdot\text{H}]^{2+}$ through π - π interaction between two neutral pbnH[•] of $[\mathbf{1}\cdot\text{H}]^{2+}$ affords $\{[\mathbf{1}\cdot\text{H}]_2\}^{4+}$, and iv) intramolecular electron and proton transfer from one pbnH[•] to another one in $\{[\mathbf{1}\cdot\text{H}]_2\}^{4+}$ results in the disproportionation reaction to afford a 1:1 mixture of $[\mathbf{1}\cdot\text{H}_2]^{2+}$ (two-electron reduced form) and $[\mathbf{1}]^{2+}$ (the starting complex).

1. Photoinduced Four- and Six-Electron Reduction of Mononuclear Ruthenium Complexes Having NAD⁺ Analogous Ligands

Mono-nuclear complexes are generally easier to synthesize and analyze their reaction mechanisms compared with multi-nuclear metal complexes. Photoinduced multi-electron redox reaction under visible light irradiation using mono-nuclear metal complexes is a fascinating approach to harvesting solar energy. Successful photochemical two electron reduction of $[\mathbf{1}]^{2+}$ drove us to investigate the photoinduced four- and six-electron reduction of $[\text{Ru}(\text{bpy})(\text{pbn})_2](\text{PF}_6)_2$ ($[\mathbf{2}]^{2+}$) and $[\text{Ru}(\text{pbn})_3](\text{PF}_6)_2$ ($[\mathbf{3}]^{2+}$), respectively, under irradiation with visible light. Photoirradiation ($\lambda > 420$ nm) of $[\mathbf{2}]^{2+}$ and $[\mathbf{3}]^{2+}$ in CH_3CN /triethanolamine (TEOA) brought about proton coupled four- and six-electron reduction of the complexes to produce $[\text{Ru}(\text{bpy})(\text{pbnH}_2)_2](\text{PF}_6)_2$ ($[\mathbf{2}\cdot\text{H}_4]^{2+}$) and $[\text{Ru}(\text{pbnH}_2)_3](\text{PF}_6)_2$ ($[\mathbf{3}\cdot\text{H}_6]^{2+}$), respectively. To elucidate the mechanism for the novel photoinduced multi-electron reduction, we examined redox and photophysical behavior of $[\mathbf{2}\cdot\text{H}_2]^{2+}$ having both pbn and pbnHH ligands. The complexes $[\mathbf{2}]^{2+}$ and $[\mathbf{2}\cdot\text{H}_2]^{2+}$ exhibit two ($E_{1/2} = -0.69$ and -0.82 V vs. SCE) and one ($E_{1/2} = -0.69$ V) reversible (pbn^{•-}/pbn) redox couples, respectively, and $[\mathbf{2}\cdot\text{H}_2]^{2+}$ and $[\mathbf{2}\cdot\text{H}_4]^{2+}$ displayed the pbnH₂



Scheme 1. Proposed mechanism for photochemical two-electron reduction of $[\mathbf{1}]^{2+}$.

localized irreversible anodic peak at 1.15 V. The metal centered Ru^{II}/Ru^{III} redox potentials of [2]²⁺, [2•H₂]²⁺ and [2•H₄]²⁺ are observed at $E_{1/2} = 1.44$ V, 1.70 V and 1.70 V, respectively. The MLCT ($d-\pi_{\text{pbn}^*}$) band of [2]²⁺ and [2•H₂]²⁺ is observed around 530 nm, and both complexes exhibit emissions from their lowest energy ³MLCT ($d-\pi_{\text{pbn}^*}$) excited states around 780 nm. The emission maximum of [2•H₂]²⁺ (786 nm) in *n*-C₄H₉CN at 77 K, and the 0–0 transition energy of the complex is determined as 1.58 eV. The excited state redox potential for the (Ru^{II*}/Ru^I) couple calculated from the equation of $E(\text{Ru}^{\text{II}*}/\text{Ru}^{\text{I}}) = E_{1/2}(\text{pbn}^{\bullet-}/\text{pbn}) + E_{\text{em}}(0-0)$ is 0.89 V. Thus, the redox potential of the (Ru^{II*}/Ru^I) couple is located at a more negative potential than that of the oxidation of pbnH₂. Photoirradiation of the MLCT ($d-\pi_{\text{pbn}^*}$) band of [2•H₂]²⁺ bearing both pbn and pbnH₂ ligands, therefore, accepts one electron through intermolecular electron transfer from TEOA to the ruthenium center without accompanying intramolecular electron transfer from pbnH₂. Indeed, the electronic absorption spectrum of [2•H₂]²⁺ in CH₃CN/TEOA (4:1, v/v) smoothly and completely changed to that of [2•H₄]²⁺ at the expense of the MLCT ($d-\pi_{\text{pbn}^*}$) absorption band at 530 nm of [2•H₂]²⁺ under irradiation with visible light ($\lambda > 420$ nm). The photoinduced four- and six-electron reduction of [2]²⁺ and [3]²⁺ in CH₃CN/TEOA, therefore, is achieved by the repeated two-electron reduction of the Ru–pbn framework as described in Scheme 1.

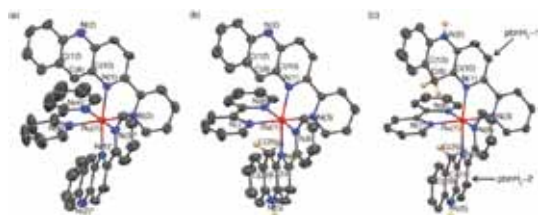


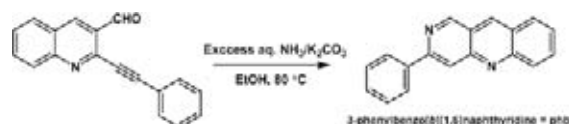
Figure 1. Crystal structures of [2]²⁺, [2•H₂]²⁺, and [2•H₄]²⁺.

2. Photochemical and Electrochemical Redox Behavior of Cyclometallated Ru(II) Complexes with NAD⁺/NADH Function

The world highly demands the renewable energy resources such as to capture and the storage of solar energy. One of the key issues for environmental science is to find out the alternative sources for the utilization of light driven energy in the form of chemical energy. In the realm of coordination chemistry ruthenium-poly-pyridyl complexes have been paid superior attention for molecular light-to-chemical energy conversion because of their unique photophysical properties and chemical stabilities. The photoinduced proton coupled “multielectronic reservoirs” of ruthenium complexes are far less common. A few research groups have reported the storage of more than one photo-excited electrons into the π^* orbital of

the poly-pyridyl ligands in the presence of sacrificial electron donors upon irradiation of visible light. Our group has developed two, four and six reversibly electron storing ability of [Ru(bpy)₂(pbn)](PF₆)₂, [Ru(bpy)(pbn)₂](PF₆)₂ and [Ru(pbn)₃](PF₆)₂ respectively, described above. We also found that [Ru(phbn)(bpy)₂](PF₆)₂ ([1]PF₆; phbn = 3-phenylbenzo[*b*][1,6]naphthyridine) undergoes photochemical proton coupled two electron reduction.

Treatment of 3-phenylbenzo[*b*][1,6]naphthyridine (phbn) obtained by Scheme 2 with [$\eta^6\text{-C}_6\text{H}_6$]RuCl₂]₂, NaPF₆ and NaOH in acetonitrile provides [Ru(phbn)(CH₃CN)₄](PF₆)₂.



Scheme 2. Synthesis of phbn.

Further addition of two equivalents of 2, 2'-bipyridyl with [Ru(phbn)(CH₃CN)₄]⁺ in 2-methoxyethanol medium gives [Ru(phbn)(bpy)₂]⁺ ([4]⁺). The complex [4]PF₆ was reduced to [Ru(phbnH₂)(bpy)₂](PF₆) ([4•HH]PF₆) by chemical, electrochemical as well as photochemical methods (Scheme 3). The reaction of [4]PF₆ with NaBH₄ in methanol/H₂O mixture (9:1 v/v) gave [4•HH]PF₆ in a very good yield. Electrolysis of [4]PF₆ at –1.15 V (vs. SCE) in CH₃CN/H₂O (9:1 v/v) also produced [4•HH]PF₆ after two equivalent of electrons were consumed in the electrolysis. The continuous photolysis at ($\lambda \geq 420$ nm) of a 0.1 mM solution of [4]PF₆ in CH₃CN/Et₃N or CH₃CN/triethanolamine (CH₃CN/TEOA) (4:1, v/v) causes a decrease in the absorption band of [4]⁺ ($\lambda_{\text{max}} = 550$ nm) and the appearance of a new species with band ($\lambda_{\text{max}} = 425$ nm) with a gradual change in color of [4]PF₆ purple to brownish red. The HR-ESI mass spectra, cyclic voltammogram as well as the UV-vis spectra of the resultant product are consistent with those of [4•HH]PF₆ obtained by the chemical reduction method. The ¹H NMR spectrum of [4•HH]PF₆ in CD₃CN displayed 17 different signals with a total intensity of 29 protons, out of which 27 are in the aromatic region generating from two bpy and phbnH₂ ligand. An AB patterned doublet observed at 3.36 (¹H, d, $J = 19.53$), 3.52 (¹H, d, $J = 18.93$) ppm due to the germinal coupling of the methylene protons.



Scheme 3. Chemical, photo, and electrical reduction of [4]²⁺.

2. Electrocatalytic Water Oxidation at an ITO Electrode Modified with Mononuclear Ruthenium Complexes²

An ITO (indium tin oxide) electrode modified with [Ru(terpy){4,4'-(CH₂PO₃H₂)₂-2,2'-bpy}(OH₂)²⁺ (**8**) was prepared to gain insight into the mechanism of O₂ evolution from water catalyzed by a series of mononuclear aquaruthenium complexes. The average separation between two closest molecules can be estimated to be ca. 35 Å. This system does not allow two or more ruthenium centers to engage in the same O₂-evolving event, and hence the electrocatalytic O₂ evolution from water promoted with this system can be fully attributable to an O₂-evolving event at a single aquaruthenium site. Indeed, the modified ITO electrode showed a clear decrease in overpotential for O₂ evolution (1.35 V in an aqueous 0.1 M Na₂SO₄/H₂SO₄ solution, pH 4.0), indicating that the O₂ evolution proceeds in a unimolecular fashion without having any intermolecular associations.



Figure 2. Schematic view of the electrochemical water oxidation catalyzed by a mononuclear ruthenium complex (**8**).

3. Photochemical Hydrogen Production from Water Catalyzed by Carboxylate-Bridged Dirhodium(II) Complexes³

A series of dinuclear Rh(II) complexes, [Rh₂(μ-OAc)₄(H₂O)₂] (HOAc = acetic acid) (**9**), [Rh₂(μ-gly)₄(H₂O)₂] (Hgly = glycolic acid) (**10**), [Rh₂(μ-CF₃CO₂)₄(acetone)₂] (**11**), and [Rh₂(bpy)₂(μ-OAc)₂(OAc)₂] (**12**), were found to serve as H₂-evolving catalysts in a three-component system consisting of tris(2,2'-bipyridine)ruthenium(II) (Ru(bpy)₃²⁺), methylviologen (MV²⁺), and ethylenediaminetetraacetic acid disodium salt (EDTA). It was also confirmed that thermal reduction of water into H₂ by MV²⁺, in situ generated by the bulk electrolysis of MV²⁺, is effectively promoted by **9** as a H₂-evolving

catalyst. The absorption spectra of the photolysis solution during the photocatalysis were monitored up to 6 h to reveal that the formation of photochemical or thermal byproducts of MV²⁺ is dramatically retarded in the presence of the Rh(II)₂ catalysts, for the H₂ formation rather than the decomposition of MV²⁺ becomes predominant in the presence of the Rh(II)₂ catalysts. The stability of the Rh(II)₂ dimers was confirmed by absorption spectroscopy, ¹H NMR, and ESI-TOF mass spectroscopy. The results indicated that neither elimination nor replacement of the equatorial ligands take place during the photolysis, revealing that one of the axial sites of the Rh₂ core is responsible for the hydrogenic activation. The quenching of Ru*(bpy)₃²⁺ by **9** was also investigated by luminescence spectroscopy. The rate of H₂ evolution was found to decrease upon increasing the concentration of **9**, indicating that the quenching of Ru*(bpy)₃²⁺ by the Rh(II)₂ species rather than by MV²⁺ becomes predominant at the higher concentrations of **9**. The DFT calculations were carried out for several possible reaction paths proposed (*e.g.*, [Rh^{II}₂(μ-OAc)₄(H₂O)] + H⁺ and [Rh^{II}₂(μ-OAc)₄(H₂O)] + H⁺ + e⁻). It is suggested that the initial step is a proton-coupled electron transfer (PCET) to the Rh(II)₂ dimer leading to the formation of a Rh(II)Rh(III)-H intermediate. The H₂ evolution step is suggested to proceed either *via* the transfer of another set of H⁺ and e⁻ to the Rh(II)Rh(III)-H intermediate or *via* the homolytic radical coupling through the interaction of two Rh(II)Rh(III)-H intermediates.

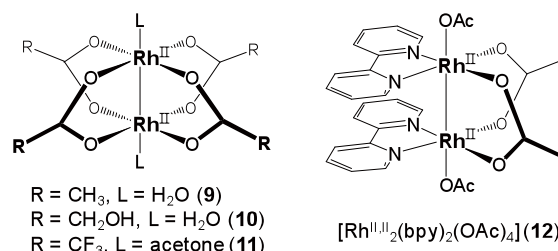


Figure 3. Structures of carboxylate-bridged dirhodium(II) catalysts for photochemical water reduction.

References

- 1) M. Yoshida, S. Masaoka, J. Abe and K. Sakai, *Chem. –Asian J.* **5**, 2369–2378 (2010).
- 2) J. Kiyota, J. Yokoyama, M. Yoshida, S. Masaoka and K. Sakai, *Chem. Lett.* **39**, 1146–1148 (2010).
- 3) S. Tanaka, S. Masaoka, K. Yamauchi, M. Annaka and K. Sakai, *Dalton Trans.* **39**, 11218–11226 (2010).

Awards

MASAOKA, Shigeyuki; The 25th Young Scholar Lectures in the 91th Annual Meeting of CSJ (2011).

KONDO, Mio; Poster Award at 60th Anniversary Conference on Coordination Chemistry in OSAKA (2010).

KONDO, Mio; The 27th Inoue Research Award for Young Scientists (2010).

* carrying out graduate research on Cooperative Education Program of IMS with Kyushu University

Visiting Professors



Visiting Professor
NISHIHARA, Hiroshi (*from The University of Tokyo*)

Coordination Programming of Electro- and Photo-Functional Materials

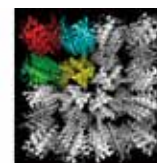
One of the goals of molecular electronics is to control electron conduction in molecular wires and networks by combining appropriate molecular units. We are investigating the construction of hetero metal complex oligomer wires by an interfacial stepwise coordination method using various combinations of surface materials, ligands and metals in order to clarify all the factors to decide the electron conduction behaviors. The surface coordination programming is being applied for development of bio-photosensors and also new types of electro- and photo-functional molecular systems based on photochromism, strong donor–acceptor interaction, π -conjugation, and molecular rotation.



Visiting Associate Professor
UENO, Takafumi (*from Kyoto University*)

Novel Functional Nano Bio-Materials Based on Protein Assembly

Our research interests focus on the understanding, utilization, and design of protein assemblies that promote chemical reactions. We are developing strategies to functionalize natural protein assemblies as well as prepare artificial protein assemblies. This will expand the possibilities of our research into several emerging fields by bringing together the fields of organic chemistry, inorganic chemistry, biochemistry, molecular biology and structural biology.



Visiting Associate Professor
OYAMA, Dai (*from Fukushima University*)

Development of Highly Functionalized Transition Metal Complexes Based on Non-Innocent Ligands

Redox reactions are one of the most fundamental chemical reactions. Nature often utilizes redox-active organics in chemical transformations. Therefore, significant attention is currently focused on ligand-centered redox reactions in transition metal complexes.

We have investigated the synthesis and properties of the ruthenium complexes containing both pyridyl binding sites and azo, naphthyridine or quinone moieties which are closely related to biologically important molecules. In particular, we have studied on some important reaction systems such as multi-electron CO_2 reductions and H_2 evolution, based on proton-coupled electron transfer (PCET).